Received: 25 January 2021 | Revised: 12 March 2021 | Accepted: 15 March 2021

DOI: 10.1002/fuce.202100002

Fuel Cells
From Fundamentals to Systems

ORIGINAL RESEARCH PAPER

Proton exchange membrane fuel cell degradation model based on catalyst transformation theory

Yunjin Ao | **Kui Chen** | **Salah Laghrouche** | **Daniel Depernet**

FEMTO-ST, UMR CNRS 6174, FCLAB, FR CNRS 3539, UBFC, UTBM, Belfort cedex, France

Correspondence
Kui Chen, FEMTO-ST, UMR CNRS 6174, FCLAB, FR CNRS 3539, UBFC, UTBM, 90000, Belfort cedex, France.
Email: kui.chen@utbm.fr

Abstract

Durability is a severe problem in the commercial application of proton exchange membrane fuel cell (PEMFC). The platinum (Pt) catalyst which greatly affects performance and durability is one of the most important components in PEMFC. However, few PEMFC degradation models focused on the Pt catalyst degradation process in molecule scale. In this paper, a novel PEMFC catalyst degradation model is developed based on the catalyst transformation theory. In this model, the Pt catalyst degrades by changing form and size according to the transformation theory, which includes Pt dissolution and Ostwald ripening mechanisms. The advantage of this new model is that the transformation of every Pt particle is calculated directly, and the characteristics of every particle are considered, thus it can give more accurate catalyst degradation process. Six groups of experimental data have been used to validate the effectiveness of the proposed degradation model of PEMFC. Furthermore, the accuracy of the proposed degradation model is superior to a traditional model, and the application of such a degradation model to the performance prediction of the PEMFC has been discussed.

KEYWORDS

experimental validation, fuel cells, Ostwald ripening, platinum dissolution, supported catalysts

1 | INTRODUCTION

Recently, public attitude toward fossil energy is becoming more negative becaues of limited supply and their traditional application is harmful to the environment. Therefore, the focus has shifted to the exploration of renewable power resources applications, such as wind power generators, solar panels, and fuel cells [1]. However, they are limited by territory and natural condition, and the manufacturing of energy conversion equipment is expensive and environmentally unfriendly [2]. Unlike other applications, hydrogen fuel cells are totally nonpolluting as the reaction product is only water [3]. Among them, proton exchange membrane fuel cell (PEMFC) has received much attention and has been widely researched [4].

Currently, the high cost and short durability of the PEMFC system are the main barriers to commercial applications [5]. For durability problem of the PEMFC system, the prognostics and health management (PHM) has played a vital role in recent years [6], as it can predict and prevent the failure before it happens [7]. The prediction of the remaining useful life (RUL) is the main aim of the prognosis of the PEMFC system. The existing prognostic models can be divided into three classes: model-driven, data-driven, and hybrid methods. Since model-based and hybrid methods are based on the physical phenomenon

List of Abbreviations: AST, accelerating stress test; CNT, carbon nanotube; CV, cyclic voltammetry; DMSO, dimethyl sulfoxide; ECSA, electrochemical surface area; MWNT, multi-walled carbon nanotube; PDF, probability density function; PEMFC, proton exchange membrane fuel cell; PHM, prognostics and health management; PRD, particle radius distribution; RUL, remaining useful life; SEM, scanning electron microscope; TEM, transmission electron microscopy; XRD, x-ray diffraction

and degradation mechanisms, it is necessary to analyze the degradation process [8].

As is well known, all layers will degrade when fuel cells operate. However, as PEMFC is a multi-scale, multi-physics, and nonlinear system, it is difficult to consider all the degradation mechanisms in all components. Among the sub-assemblies of PEMFC, the durability problem of the electrocatalyst layer is more serious and more decisive than other layers [9]. Therefore, the focus of this paper is on the degradation of the catalyst layer. The degradation of the catalyst layer is governed by the catalyst transformation theory that includes three paths: the carbon support corrosion and falling apart, platinum particle taking off, and platinum particle coarsening [10,11]. However, as the mechanism of carbon corrosion in catalyst is still unclear, the factors that affect the durability of carbon support are still unknown [12,13]. Therefore, it is difficult to find a quantitative model to distinguish the Pt particle degradation caused by support corrosion or transformation. Thus most research works focus on the particle coarsening process [14,15].

Several experiments focusing on the degradation mechanisms of Pt catalyst have been carried out, and the main experimental method is the accelerating stress test (AST) [16]. Researchers built different reaction systems and then measured the catalyst transformation process [13]. The main measuring methods include: (i) scanning electron microscope (SEM) and transmission electron microscopy (TEM), which show the images of Pt particles and catalyst surface, and the Pt particle radius distribution (PRD) evolution can also be detected; (ii) cyclic voltammetry (CV), which shows the electrochemical surface area (ECSA) of catalyst; and (iii) x-ray diffraction (XRD), which gives information about particle composition and structure. The catalyst PRD is a direct representation of the coarsening degree of a group of Pt particles, and the ECSA is the active surface that is effective for the reactions. So it is very important to obtain the PRD and ECSA of a catalyst, so that the health state of the PEMFC can be monitored [17].

At the same time, the degradation mechanisms were also studied by theory analysis. Several researchers tried to build mathematical models in different scales [18]. Tang et al. studied the stability of nanoparticles using thermodynamic analysis. They constructed a diagram that gave the Pt reaction potential dependent on particle size and pH value of the solution, and some thermodynamic parameters were discussed [19]. Ryosuke et al. calculated the degradation of Pt particles with and without carbon supports by a first principle method [20]. It was shown that the reaction potential at edges was lower than those at flat surfaces, which leads to the vulnerability of edges.

The widely confirmed catalyst transformation mechanisms are Pt dissolution and Ostwald ripening [21]. Pt dissolution mechanism has been researched for a long time. In [22], the experiment was carried out under potential cycling between different voltage ranges, and the relationship between Pt dissolution and ECSA degradation was obtained. In another experiment [23], the content of Pt during the experiment was detected by inductively coupled plasma mass spectrometry (ICP-MS), and the possible Pt dissolution mechanisms were proposed. In [18], it was also researched using the first principle calculation. Here, the authors studied the effect of particle shape on Pt dissolution and ranked the stability of different shapes.

Pt particle Ostwald ripening mechanism has also been researchedlong ago [24]. Ostwald ripening is a common phenomenon in metal material, and it is also found in Pt catalyst [25]. The phenomenon describes the transition of the disperse phase, in which the size distribution changes with a shift toward larger particle size [26]. In [27], the authors researched the Ostwald ripening of Pt nanoclusters with atomic control of initial size distribution, and mono-dispersed clusters were found to be more stable compared to the bimodal initial size distribution. It was also researched by theoretical calculation in [28]. Focusing on Ostwald ripening of platinum nanoparticles supported on titanium dioxide (TiO_2), the authors found that the ripening was very sensitive to the structure of oxide facets and crystal phases. Y. D. Smet et al. [29] used a molecule scale model with Ostwald ripening to get the pattern of Pt PRD evolution, but it was not verified by experiment.

However, there is little research on the PEMFC degradation model based on the catalyst degradation process, which can be used as the basis of prognosis. A model about the degradation of Pt catalyst was put forward in [30], but only chemical dissolution was analyzed. Moreover, the Pt particles were treated as a whole, thus the characteristic of particles was not considered. To overcome those disadvantages, a PEMFC degradation model is built in this paper based on the Pt particle transformation theory. In the model, a system with a group of Pt particles is created to model the degradation process of PEMFC catalyst. These particles gain or lose molecules one by one according to the predetermined transformation mechanisms, i.e., Pt dissolution and Ostwald ripening mechanisms. After degradation, the molecule number and radius of every particle in the system can be counted, thus the PRD and ECSA of the system can be obtained, which is important for the health state assessment of PEMFC. The advantage of the proposed method is that the dynamic transformation of every Pt particle is directly calculated according to their characteristics. The main contributions of this paper are:

(i) A novel PEMFC degradation model is proposed based on the catalyst transformation theory, which considers both the Pt dissolution and Ostwald ripening

mechanisms. The proposed model can calculate the size change of Pt particles during the operation, thus reveals the health state of the catalyst.

(ii) The proposed PEMFC catalyst degradation model is verified by six groups of experimental data, and the PRD and ECSA calculated by the proposed model are very close to the experiment result.

(iii) Compared with traditional analytical model, the proposed PEMFC catalyst degradation model has higher accuracy. The proposed method considers more catalyst degradation mechanisms, thus it is more accurate.

(iv) The method to apply the proposed PEMFC catalyst degradation model to forecasting long-term PEMFC degradation is put forward. Therefore, the proposed model can be helpful to the degradation prediction and prognosis of PEMFC.

The paper is organized as follows: In Section 2, the proposed PEMFC catalyst degradation model is described in detail. In Section 3, the result of the model is verified by experiments and compared with other model, to show its reliability and advantage. In Section 4, the discussion about the application of the proposed model is presented. Finally, the major conclusions are summarized in Section 5.

2 | MOLECULE SCALE CATALYST DEGRADATION MODEL

In this section, the details of the molecule scale Pt catalyst degradation model are presented. First, the framework of the model is given, and the programming process is addressed in Section 2.1. Then, the Pt dissolution and Ostwald coarsening mechanisms are explained in Section 2.2 and 2.3 respectively, as they play important roles in the degradation model.

2.1 | Basic idea of Pt catalyst degradation model

There were some analytical solutions for Pt dissolution, and they tried to treat all of the particles as a whole [30]. However, in the Pt catalyst system, every particle has different parameters that cannot be equalized, such as the reaction potential and the coverage of PtO on the particle surface [31]. Therefore, it is a better choice to calculate every particle respectively [32].

A group of Pt particles in a catalyst system can be calculated one by one, and then the feature of the system can be counted. Suppose there are M particles, each particle i contains $n_{i,0}$ Pt atoms at the beginning, and the radius of the particle is $r_{i,0}$ according to a predetermined distribution. The total number of the particles are set as M, and it is decided by the Pt system scale that we want to simulate. The higher is M, the smoother is the particles size distribution and more accurate is the simulation. However, too much particles will need several computational sources to simulate the system. In this work, the M is set as 140,000, so that to get a balance between the computational burden and accuracy. At time step j, the particles exchange atoms with each other or with environment, according to the function shown as Equation (1). Thus, the particle distribution transforms as time goes on:

$$n_{i,j} = n_{i,j-1} + \Delta t \cdot \sum \upsilon\left(r_{i,j}\right) \tag{1}$$

where Δt is the time step length; $\upsilon(r_{i,j})$ is the velocity of reactions that gain or lose atoms on Pt particles, which is a function of particle radius. After the molecule number of each particle has been obtained, as the particles are all supposed to be sphere, the new particle radius of the particle can be calculated according to the molecule number and molecule volume.

Theoretically, all the reactions that cause loss or gain of Pt atoms should be considered in $\upsilon(r_{i,j})$. However, although several Pt coarsening mechanisms have been proposed, many of them are still uncertain, far from quantitative calculation. Therefore, we consider only Pt dissolution and Ostwald ripening in this paper, as the mechanisms are widely confirmed.

Several research show that the Pt particle dissolution is one of the main paths that cause particle radius transformation [33]. According to Ref. [32], there exist two kinds of reactions, i.e., electrochemical dissolution as shown in Equation (2) and chemical dissolution as shown in Equation (3) and Equation (4). The diagrams of electrochemical dissolution and chemical dissolution are both shown in Figure 1. Several experiments have confirmed that the electrochemical path is more severe when the electric potential is high, while the chemical dissolution plays the leading role when the catalyst is in acid oxidizing environment. Some researchers showed that the reaction products could be PtO_2, but the experiments have confirmed that it takes only a small percentage in the system [32]. Therefore, it is not considered in this paper:

$$\mathrm{Pt} \overset{k_1}{\leftrightarrow} \mathrm{Pt}^{2+} + 2e^- \tag{2}$$

$$\mathrm{Pt} + \mathrm{H_2O} \overset{k_2}{\leftrightarrow} \mathrm{PtO} + 2\mathrm{H}^+ + 2e^- \tag{3}$$

$$\mathrm{PtO} + 2\mathrm{H}^+ \overset{k_3}{\leftrightarrow} \mathrm{Pt}^{2+} + \mathrm{H_2O} \tag{4}$$

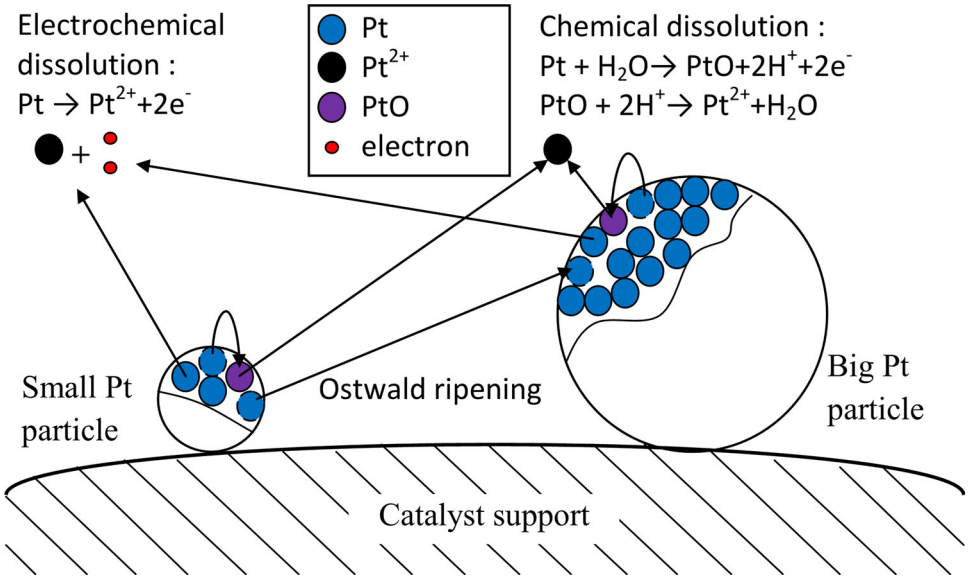

FIGURE 1 Diagram of platinum (Pt) particle coarsening mechanisms: platinum (Pt) dissolution and Ostwald ripening

The Pt dissolution and Ostwald ripening velocity will decide the Pt number of particles, so they are plugged into Equation (1). The transformation rules of Pt atoms numbers on every particle is shown as Equation (5). At the same time, the PtO is produced during the chemical dissolution process, so there exist PtO molecules on particles. The PtO molecules number $m_{i,j}$ on particle i at time step j can be calculated by Equation (6):

$$n_{i,j} = n_{i,j-1} + \Delta t \left(-\upsilon_1\left(r_{i,j}\right) - \upsilon_2\left(r_{i,j}\right) + \upsilon_{or}\left(r_{i,j}\right)\right) \quad (5)$$

$$m_{i,j} = m_{i,j-1} + \Delta t \left(\upsilon_2\left(r_{i,j}\right) - \upsilon_3\left(r_{i,j}\right)\right) \quad (6)$$

where υ_1, υ_2, υ_3 are the velocities of reactions (2), (3) and (4), respectively, and υ_{or} is the velocity of atoms gain or lose by Ostwald ripening.

If both $n_{i,j}$ and $m_{i,j}$ equal to 0, it means that this particle has totally dissolved. By counting the number of particles whose radii are in a certain range, the PRD can be obtained. Also, we can get the ECSA of the system by summing the surface area of all particles. This model can be easily reformed if other degradation mechanisms are included.

In summary, the process of the model can be shown as Figure 2. The steps are as follows:

(i) A group of particles is created, according to a known probability density function (PDF) fitted by experimental data, such as Gaussian distribution and log-normal distribution. In this research, as there is a long tail toward big particles in the distribution, a log-normal distribution is chosen, and the least square fitting method is applied.

(ii) The velocities of Pt dissolution and Ostwald ripening are calculated for every particle, according to the Pt dissolution mechanism given in Section 2.2 and Ostwald ripening mechanisms in Section 2.3.

(iii) The remaining amount of Pt atoms and PtO on every particle can be obtained according to Equations (5) and (6), respectively. Some particles may lose all the atoms and disappear, so the total number of particles will decrease.

(iv) The operation time is checked. If it is smaller than the total time, go back to step 2 and 3 to continue the degradation process. Otherwise, if the total time of the process is reached, we can go to step 5 to show the result.

(v) Finally, the features of the system are counted and plotted, usually in the form of PRD and ECSA. Using this method, we can monitor the degradation process and describe the performance of the system.

2.2 | Pt dissolution mechanism

The Pt dissolution mechanisms and velocities $\upsilon_1, \upsilon_2, \upsilon_3$ are explained in this part. By thermodynamic analysis, smaller the particle is, more violent the reaction will be [33]. For every particle, the equilibrium electrode potential is the function of the particle radius, thus the reaction velocity is also different. The velocity of reaction (2) can be calculated by Equation (7):

$$\upsilon_1\left(r_{i,j}\right) = \left(1 - \theta_{i,j-1}\right)\ k_1\left(r_{i,j-1}\right) \exp\left(\frac{F\left(E - E_1\left(r_{i,j-1}\right)\right)}{2RT}\right) \quad (7)$$

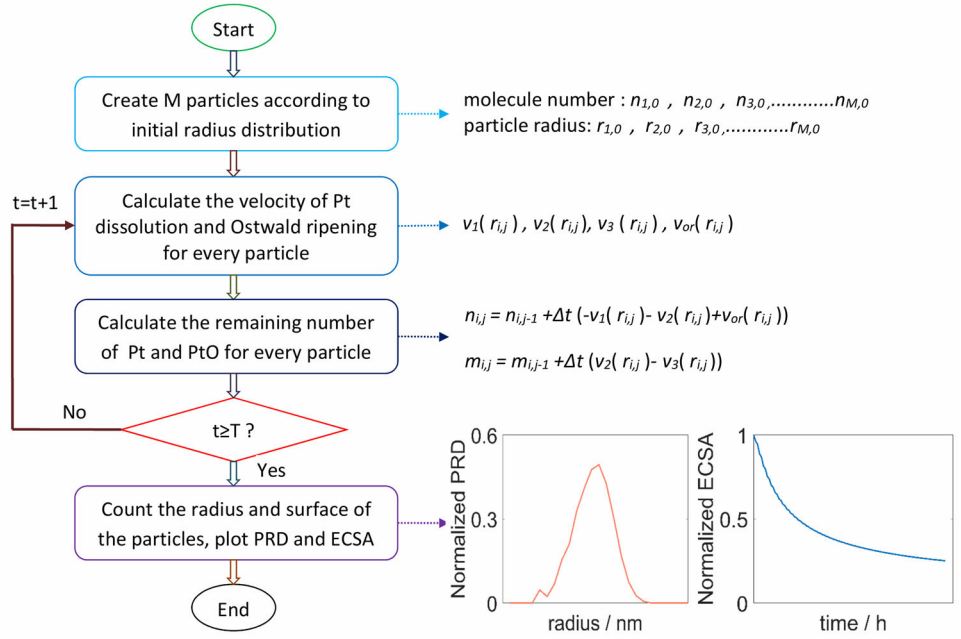

FIGURE 2 Diagram of the programming process of molecule scale degradation model

where

$$k_1\ (r_{i,j-1}) = k_1^{\infty} \exp\left(\frac{\beta\gamma V_{pt}}{RTr_{i,j-1}}\right) \tag{8}$$

$$E_1\ (r_{i,j-1}) = E_1^{\infty} - \frac{2\beta\gamma V_{pt}}{Fr_{i,j-1}} \tag{9}$$

where $v_1(r_{i,j})$ is the velocity of Equation (2) for particle i at time step j; $\theta_{i,j-1}$ is the fraction of particle surface covered by PtO, this is calculated for every particle at every time step; $k_1(r_{i,j-1})$ is the equilibrium rate constant of Equation (2) for particle i, and it is a function of the particle radius as shown in Equation (8); F is Faraday constant, the value is 96,485 C mol^{-1}; E is the electric potential imposed on the cathode, which is decided by the experiment condition; $E_1(r_{i,j-1})$ is the equilibrium potential of Equation (2), which is a function of the particle radius as Equation (9); R is the ideal gas constant, the value is 8.314 J mol^{-1} K^{-1}; T is the temperature of environment, and it is decided by the experiment condition; k_1^{∞} is the equilibrium rate constant of Equation (2) for Pt bulk, and it is a tuning parameter; β is a proportional constant between 0 and 1; γ is the interfacial surface tension of Pt, and $\beta\gamma$ is taken as effective surface tension, it is set as 1.2 J m^{-2} according to Ref. [26]; V_{pt} is the molar volume of Pt, the value is 9.09 $\times 10^{-6}$ m^3 mol^{-1} (20°C); E_1^{∞} is the equilibrium potential for Pt bulk, it is 1.188 V according to Ref. [34].

It can be seen that the electrochemical dissolution velocity is affected by several factors. The coverage of PtO on particle surface will decide the contact possibility of molecules and external environment. The equilibrium rate constant reveals the nature of the reaction. The external potential will rise the reaction energy, while the equilibrium potential shows the basic energy needed for the reaction.

For reaction (3), the velocity can be given as Equation (10). This equation declares the velocity of Pt atoms to transform into PtO molecules. Usually the PtO molecules cover on the surface of Pt particles and protect Pt from corrosion. However, the PtO itself will dissolve under acidic environment. Therefore, the reaction (3) does not lead to Pt dissolution directly, but it achieves the same effect. The velocity of Equation (3) is also affected by coverage of PtO, equilibrium rate constant, external potential and equilibrium potential:

$$v_2(r_{i,j}) = (1-\theta_{i,j-1})\ k_2\ (r_{i,j-1}) \exp\left(\frac{F\ (E - E_2\ (r_{i,j-1}))}{2RT}\right) \tag{10}$$

where

$$k_2(r_{i,j-1}) = k_2^{\infty} \exp\left(\frac{\beta\gamma V_{pt}}{RTr_{i,j-1}}\right) \tag{11}$$

$$E_2(r_{i,j-1}) = E_2^{\infty} - \frac{2\beta\gamma V_{pt}}{Fr_{i,j-1}} \tag{12}$$

where $v_2(i,j)$ is the velocity of Equation (3) for particle i at time j; $k_2(r_{i,j-1})$ is the reaction constant of Equation (3)

for particle i, given as Equation (11); $E_2(r_{i,j-1})$ is the equilibrium potential of Equation (3), given as Equation (12); k_2^{∞} is the equilibrium rate constant of Equation (3) for Pt bulk, it is also a tuning parameter; E_2^{∞} is the equilibrium potential of Equation (3) for Pt bulk, and it is 0.98 V [34].

The velocity of reaction (4) is given as Equation (13). Unlike the velocity of reactions (2) and (3), reaction (4) is not affected by external electric potential, as it is just a chemical reaction without the participation of electrons. It is affected by PtO coverage, reaction rate constant, and pH level:

$$v_3(r_{i,j}) = \theta_{i,j-1}\, k_3\left(r_{i,j-1}\right) \frac{c_{H^+}}{c_{H^+}^{\mathrm{ref}}} \tag{13}$$

where

$$k_3(r_{i,j-1}) = k_3^{\infty} \exp\left(\frac{\beta\gamma V_{pt}}{RTr_{i,j-1}}\right) \tag{14}$$

where $v_3(i,j)$ is the velocity of Equation (4) for particle i at time j; $k_3(r_{i,j-1})$ is the equilibrium rate constant of Equation (4) for particle i, given as Equation (14); k_3^{∞} is the equilibrium rate constant of Equation (4) for Pt bulk, it is a tuning parameter; c_{H^+} is the concentration of H^+ in the solution, which is decided by the experiment condition; $c_{H^+}^{\mathrm{ref}}$ is the reference value of c_{H^+}, which is set as 1 mol L^{-1} in this work.

Using these equations, the velocity of Pt dissolution can be calculated according to the experimental environment, and it varies for different particle radius. The details about the derivation process of Pt dissolution can be found in [30].

2.3 | Ostwald ripening mechanism

Except for the Pt dissolution, several researchers reported the Ostwald ripening process of Pt particles [25, 26]. The phenomenon of Ostwald ripening can happen in all two-phase systems, including liquid–liquid, liquid–solid, and solid–solid mixture, and it has been researched for several decades [35]. It is a common process in almost all metal crystals, and the system is not equilibrium as the chemical energy is different for big particles and small particles. In Ostwald ripening, a very important driven force is the interfacial energy, so the particles change their shape or coarsen to reduce the specific area. The process is controlled by the diffusion of material; Greenwood [36], Lifshitz and Slyozov [37], and Wagner [38] (LSW theory) have studied the feature of Ostwald ripening process and given the diffusion controlled mechanism.

The Ostwald ripening process is also shown in Figure 1, and the Pt atoms transfer from small particles to big particles. The velocity of Ostwald ripening can be given as Equation (15) [29]. It can be seen that when the radius of a particle is smaller than the mean radius, the particle will lose atoms. Otherwise, the atoms will gather on the bigger particles, thus the Pt particles coarsen:

$$v_{or}(r_{i,j}) = 4\pi D_m c_{Pt}\alpha\left(\frac{r_{i,j}}{\overline{r_j}} - 1\right) \tag{15}$$

where $v_{or}(r_{i,j})$ is the velocity of Ostwald ripening for particle i at time step j; D_m is the diffusion coefficient of Pt, it is a tuning parameter; c_{Pt} is the concentration of Pt atoms, which is set as 10^{-6} mol L^{-1} [19]; α is a material decided constantly in the order of 1 nm, it is set as 1 [29]; $\overline{r_j}$ is the mean radius of all particles, it is calculated at every time steps.

Other mechanisms about Ostwald ripening were also reported such as electrochemical Ostwald ripening, which happens by ionization. However, it is not confirmed yet, thus it is not considered in this paper.

3 | VERIFICATION AND COMPARISON

Several experiments focusing on the durability of Pt catalyst under different operation conditions have been carried out. In those experiments, the Pt catalyst was put in solution to proceed AST for a certain time. After AST, the catalyst was measured by different methods such as TEM and CV. Using TEM, the PRD can be observed and plotted, which is very important for analyzing the particle transformation process. To have a unified criterion to compare the PRD at different scales, the PRD is normalized, i.e., the particle numbers of all different radii are divided by the maximum particle number, so that to compare the relative change of the particle size distribution. Using CV, the ECSA can be measured during the experiments, and it is an important indicator for the performance of fuel cells.

In this section, the model addressed above is applied to different experimental cases. First, the model is verified by two experiments, where different electric potential is imposed to the carbon supported catalyst. Then, the result of this model is compared with other models, based on two other experimental cases.

As addressed above, the parameters used in our research can be divided into three categories. First, constant parameters that are given below the equations in Section 2.2 and 2.3. Second, experimental condition parameters that are decided by experimental condition, such as concentration c_{H^+}, imposed electric potential E and experiment temperature T. Third, tuning parameters k_1^{∞}, k_2^{∞}, k_3^{∞}, and

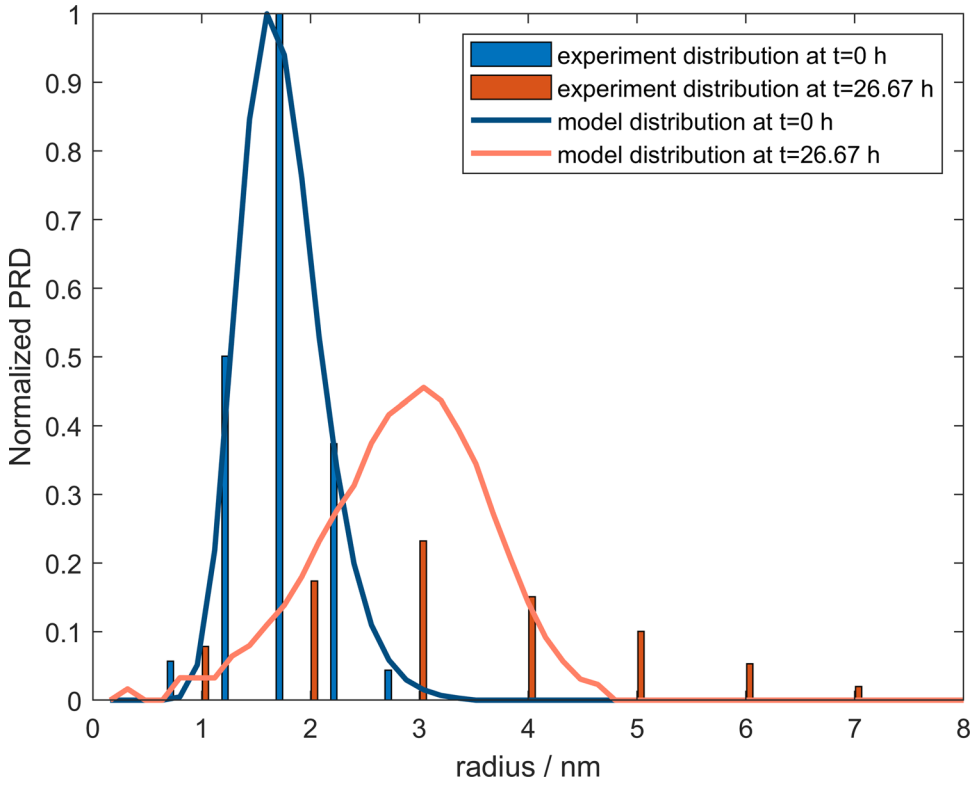

FIGURE 3 Normalized particle radius distribution (PRD) transformation of model and experiment data of Zhang et al. [40]

TABLE 1 The parameters used in the model for the experiment of Zhang et al. [40]

Parameter	Value
E (V)	1.5
c_{H^+} (mol L^{-1})	0.1
T (K)	298
k_1^∞ (s^{-1})	10^{-8}
k_2^∞ (s^{-1})	10^{-9}
k_3^∞ (s^{-1})	10^{-2}
D_m (L mol^{-1} s^{-1})	2×10^4

the diffusion coefficient D_m. For every experiment case, the experimental condition parameters and tuning parameters are given when the result of the proposed model is compared with the experiment.

3.1 | Experimental verification case 1

The material of catalyst support and the operating electric potential are the most studied two variables. Several research works have discussed the effect of electric potential [39]. The high electric potential condition usually happens when the power output is low, and the potential is close to open circuit potential.

Zhang et al. carried out an ex situ experiment under constant electric potential (1.5 V) in a 0.1 mol $L^{-1}HClO_4$ solution for 26.67 h [40]. In the experiment, they used a fuel cell that included a glassy carbon working electrode, an Ag/AgCl reference electrode, and a Pt wire counter electrode. Three different experiments were carried out under potential cycles of different range, and we just use the result under constant potential in this study. The process was detected by different methods, more details about the experiment can be found in [40]. The parameters used in this case are shown as Table 1. The result of the model is compared with the experiment as shown in Figure 3.

The initial distribution of model is fitted as log-normal distribution by experiment, and it corresponds well with the experiment. The mean radius is 3 nm for both model and experimental data after 26.67 h, which proves that this model is reliable. There are also some differences. After degradation, there are more big particles for the experimental result, while for model result the distribution finishes when the particle radii is bigger than 5 mm. This could be the result of some unknown coarsening mechanisms which are not considered in the model. It is possible that there exist some driven forces between big particles, so that two big particles join as one directly. However, these mechanisms are not confirmed. The proposed model can give distribution with the same peak position, so it is acceptable.

TABLE 2 The parameters used in the model for the experiment of Parthasarathy et al. [41]

Parameter	Value
E (V)	0
T (K)	298
k_1^{∞} (s^{-1})	10^{-8}
D_m (L mol^{-1} s^{-1})	1.5×10^4

3.2 | Experimental verification case 2

Another experiment was carried out by Parthasarathy et al. [41]. This experiment happened in N2-purged 0.1 mol L^{-1} $PtCl_4$ solution in dimethyl sulfoxide (DMSO), and the external potential was set as 0 V. In their work, they studied the degradation of both Pt and Ag particles on carbon by putting the catalyst in different solution. The powder samples were removed and detected after 1 day, 3 days, 5 days, and 7 days, and the result was analyzed and compared. The details can be found in Ref. [41].

In this case, as the solvent used in the experiment is organic liquid, the Pt chemical dissolution path by Equations (3) and (4) cannot happen because there is no water. Therefore, only the parameters of Pt electrochemical dissolution and Ostwald ripening are needed in the model. The parameters used in this case are shown in Table 2.

The model and experimental results are shown in Figure 4. It can be seen that the initial distribution of the experiment is also fitted by log-normal distribution, and the mean radius of particles is very small. After degradation, the model result corresponds well with the experiment at 5 days, but there are some differences between model and experimental result for other time. At the beginning, the particle transformation of the model is quicker than experiments, like at 1 day and 3 days, as there are more bigger particles in the model result. On the contrary, the degradation of model is slower than experiments at 7 days, as the particle size of model is smaller than the experiment. This could be caused by the extremely small initial radius of the system. In our model, the molecule transportation from small particles to big particles is emphasized, thus the reaction is quick when there are many small particles at the beginning. Later, the transformation calculated by model slows down, as the small particles have already been consumed. However, the transformation velocity of experiment is almost the same during the process. The difference may be caused by some unknown mechanisms, in which the particle transportation is always remarkable regardless of the particle size. However, the proposed model can give approximate results, which could provide reference for the tendency of Pt degradation.

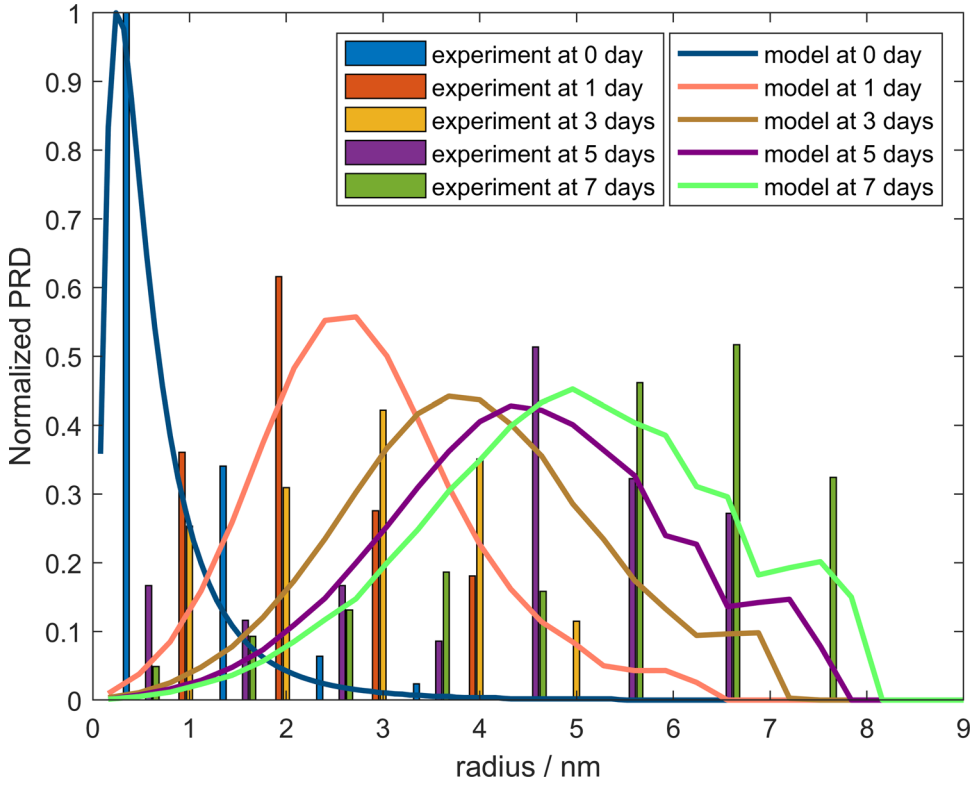

FIGURE 4 Normalized particle radius distribution (PRD) transformation of model and experiment data of Parthasarathy et al. [41]

3.3 | Comparison with analytical Pt degradation model

Rinaldo et al. built a model with an analytical solution for the degradation of Pt catalyst [30]. In their model, they only considered Pt chemical dissolution, and the equations were obtained by analyzing the velocity of reactions. The model is given as Equations (16)–(18), which shows the relationship between the number of particles and particle radius at a certain time. Their model was applied to two experiments, thus we use the model of this work in the same experiments, and the results were compared:

$$\frac{\partial f(\xi,\tau)}{\partial \tau} + \xi^2 \exp(\xi)\ \frac{\partial f(\xi,\tau)}{\partial \xi} = -\xi^2 \exp(\xi) f(\xi,\tau) \tag{16}$$

where

$$\xi = \frac{R_0}{r} \quad R_0 = \frac{2\beta\gamma V_{\mathrm{Pt}}}{RT} \tag{17}$$

$$\tau = \frac{t}{T_0} \quad T_0 = \frac{2\beta\gamma}{RTk_3^{\infty}} \tag{18}$$

where f is the number of particles of a certain radius; r is the radius of the particle; t is the time of the dissolution progress; R_0 and T_0 are the overall coefficients which can be called the characteristic radius and characteristic time, respectively; ξ and τ are dimensionless radius and dimensionless time, respectively. By the method of characteristics, solution of Equation (16) can be given as:

$$f(\xi,\tau) = f_0(\xi_0)\exp(-(\xi-\xi_0)) \tag{19}$$

$$Ei(1,\xi) - \frac{\exp(-\xi(\tau))}{\xi(\tau)} = \tau + Ei(1,\xi_0) - \frac{\exp(-\xi_0)}{\xi_0} \tag{20}$$

where Ei is the exponential integral function and ξ_0 is the initial value of ξ. By Equations (19) and (20), the transformation of PRD in the whole dissolution progress can be obtained for given initial PRD. More details about the model can be found in [30].

Compared with the model built by Rinaldo et al., the model proposed in this paper is superior in two aspects. First, the proposed model considers more Pt transformation mechanisms. Pt electrochemical dissolution, chemical dissolution, and Ostwald ripening velocities are all applied in our model, while only chemical dissolution is considered in their model. Moreover, by the method proposed in this research, the Pt transformation is obtained one particle by one particle, while in their model the particles are represented in several groups. Therefore, in our research the particle radius distribution is continuous, which is closer to the reality.

TABLE 3 The parameters used in the model for the experiments of Shao et al. [42]

Parameter	Value of Pt/C	Value of Pt/CNT
E (V)	1.2	1.2
c_{H^+} (mol L^{-1})	1	1
T (K)	298	298
k_1^{∞} (s^{-1})	10^{-7}	10^{-9}
k_2^{∞} (s^{-1})	10^{-8}	10^{-10}
k_3^{∞} (s^{-1})	10^{-2}	10^{-4}
D_m (L mol^{-1} s^{-1})	5×10^2	1.5×10^2

The model of Rinaldo et al. was applied to the experiment of Shao et al. [42], where the same accelerating stress test was carried out for Pt catalyst supported by carbon black (Pt/C) and Pt catalyst supported by carbon nanotubes (Pt/CNT), respectively. The catalyst was put in 0.5 mol $L^{-1}H_2SO_4$ solution, and the durability of Pt/C and Pt/CNT was compared. In the experiments, the sample was self-made, and TEM and XRD were applied to analyze the result. More details can be found in [42]. The parameters used in this case are shown in Table 3. The PRD of Pt/C and Pt/CNT is obtained and shown in Figures 5 and 6, respectively. The result of the model built by Rinaldo et al. is also shown in Figure 5.

It can be seen that the result of this model is more centralized than the experiment, but the mean radius corresponds well with the experiment. Meanwhile, the Pt/CNT is more durable than Pt/C, which is the same as the conclusion of the experiment. By comparing the result of the model of this paper and that of Rinaldo, we can see that the result of this model is accurate for small particles, but neither model works well for big particles. This could be the result of the production process of the Pt sample used in the experiment, as the process greatly affects the adhesion of Pt particles on the support.

At the same time, the ECSA of the experiment and model are shown in Figure 7. And the mean ECSA degradation rate of experiments and the model are shown in Table 4. ECSA is a key parameter to characterize the performance and durability of the catalyst. It can be seen that the ECSA degradation of the proposed model and experiment has the same tendency, and the ECSA degradation of Pt/CNT is much slower than that of Pt/C. For Pt/CNT, the calculated ECSA degradation is a little smaller than the result of experiment, and this may be caused by the underestimation of big particles number in the model. For Pt/C, the error between the model and the experiment result is relatively significant at the beginning, and it decreases with time, which is caused by different degradation rate of the model and the experiment at the beginning. The relative error of mean ECSA degradation rate is not more than 13% for both cases, so the model result is acceptable.

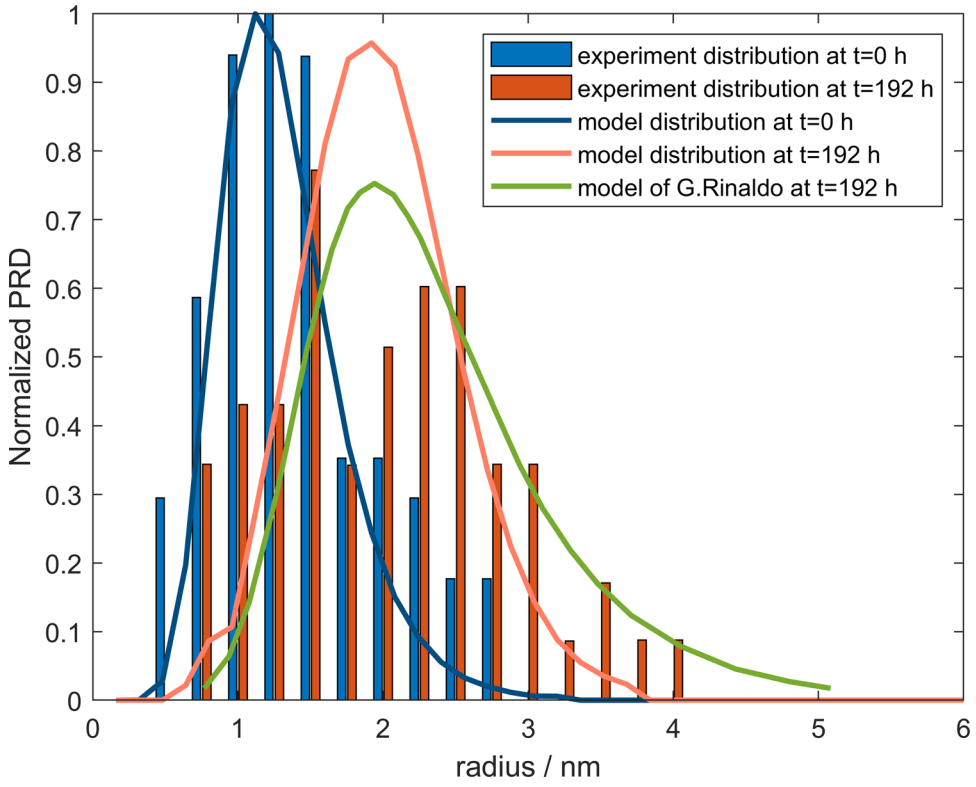

FIGURE 5 Normalized particle radius distribution (PRD) transformation of models and experiment of Shao et al. [42] for Pt/C

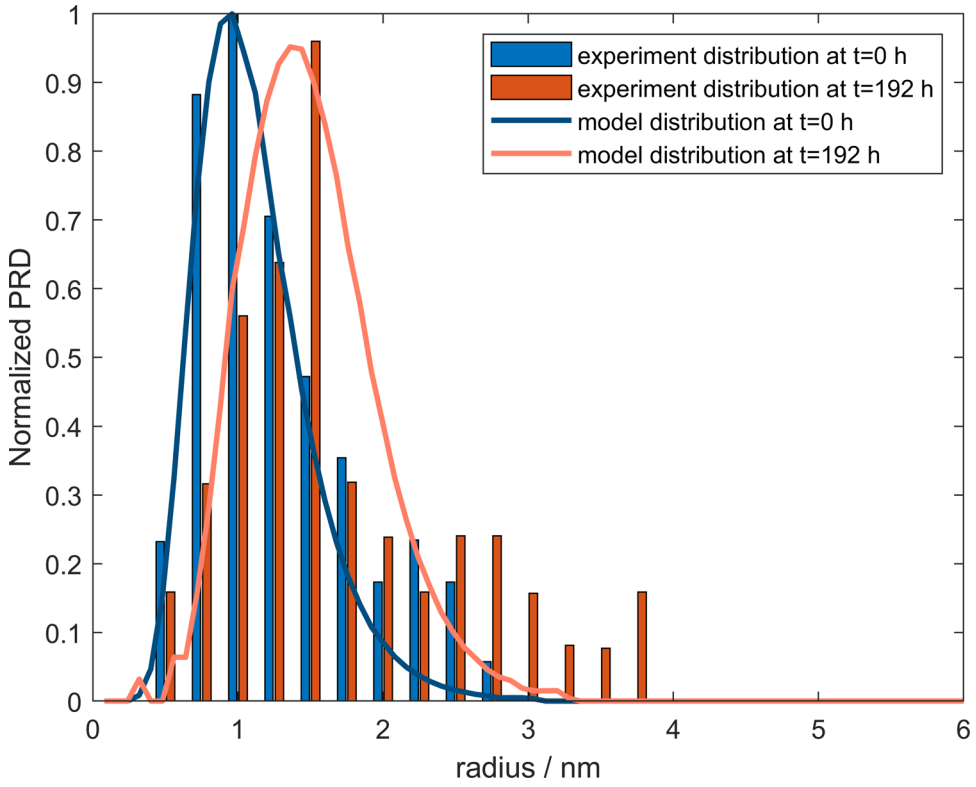

FIGURE 6 Normalized particle radius distribution (PRD) transformation of models and experiment of Shao et al. [42] for Pt/CNT

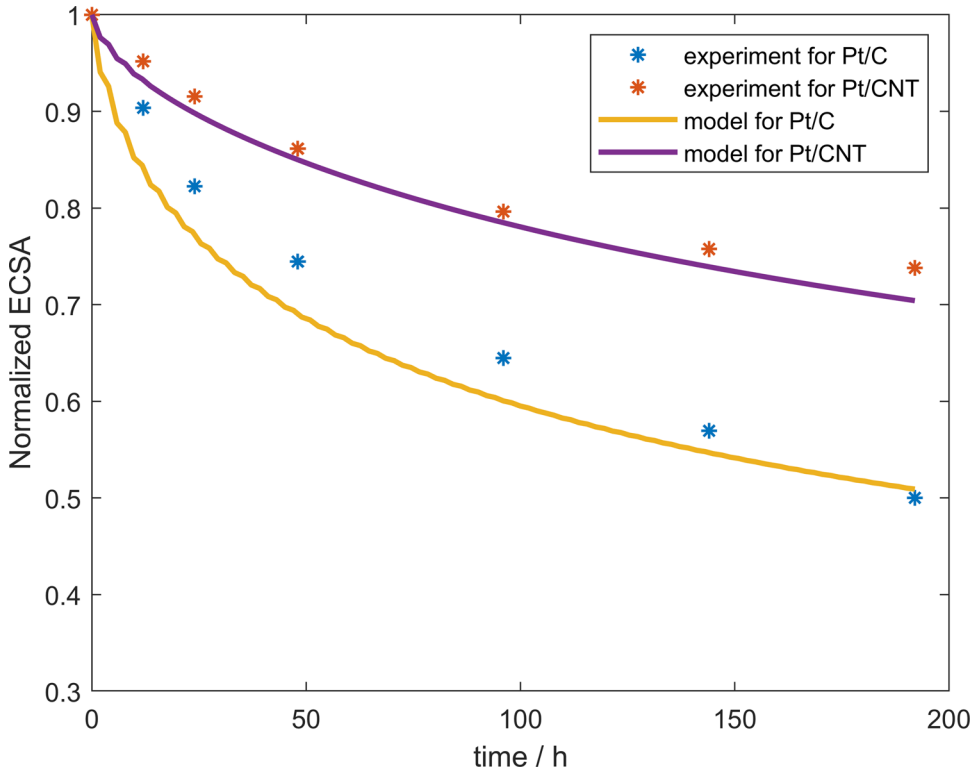

FIGURE 7 Normalized electrochemical surface area (ECSA) of model and experiment of Shao et al. [42] for Pt/C and Pt/CNT

TABLE 4 Mean electrochemical surface area (ECSA) degradation rate of model and experiment of Shao et al. [42]

Material	Experiment (h^{-1})	Model (h^{-1})	Relative error
Pt/C	0.0026042	0.0025562	9.82%
Pt/CNT	0.0013640	0.0015409	12.97%

TABLE 5 The parameters used in the model for the experiments of Wang et al. [43]

Parameter	Value of Pt/Vulcan XC72	Value of Pt/MWNT
E (V)	0.9	0.9
c_{H^+} (mol L^{-1})	1	1
T (K)	333	333
k_1^∞ (s^{-1})	3×10^{-4}	10^{-5}
k_2^∞ (s^{-1})	2×10^{-5}	10^{-6}
k_3^∞ (s^{-1})	4×10^{-2}	10^{-3}
D_m (L mol^{-1} s^{-1})	10^3	2×10^2

Another experiment was also compared with the model built by Rinaldo et al. The experiment was carried out by Wang et al., focusing on the comparison of Pt supported by Vulcan XC-72 (Pt/Vulcan XC-72) and multi-walled carbon nanotube (MWNT) [43]. Vulcan XC-72 is a kind of furnace carbon black which is widely used, while MWNT is an emerging material as catalyst support. The electrochemical measurement was carried out in a three-electrode electrochemical fuel cell, by a rotating disk electrode setup with an Ag/AgCl reference electrode and a Pt wire counter electrode. The catalyst was put in N_2 purged 0.5 mol $L^{-1}H_2SO_4$ solution, with external constant potential 0.9 V. The experiment was carried out under thermostatic environment of 60°C. More details about the experiment can be found in [43]. The parameters used in this case are shown in Table 5.

The PRD of Pt supported by Vulcan XC-72 and MWNT are shown in Figures 8 and 9, respectively. The model of Rinaldo was also carried out for this experiment, and the result is shown in Figure 8. It can be seen that the catalyst supported by Vulcan XC-72 degrades quickly, while there is only a little degradation for Pt/MWNT, which shows that the Pt/MWNT catalyst is much more durable than Pt/Vulcan XC-72. The result of this model is close to the experiment. In Figure 8, the result of the model of Rinaldo does not correspond well with the experiment, while the proposed model is closer to the experiment. Therefore, the proposed model of this paper is more accurate than the analytical model. The reason why the proposed model is more accurate is that the Ostwald ripening is considered in our model, as it accelerates the atoms transportation between small particles and big particles.

In Figure 9, the model proposed in this paper also corresponds well with the experimental results for Pt/MWNT.

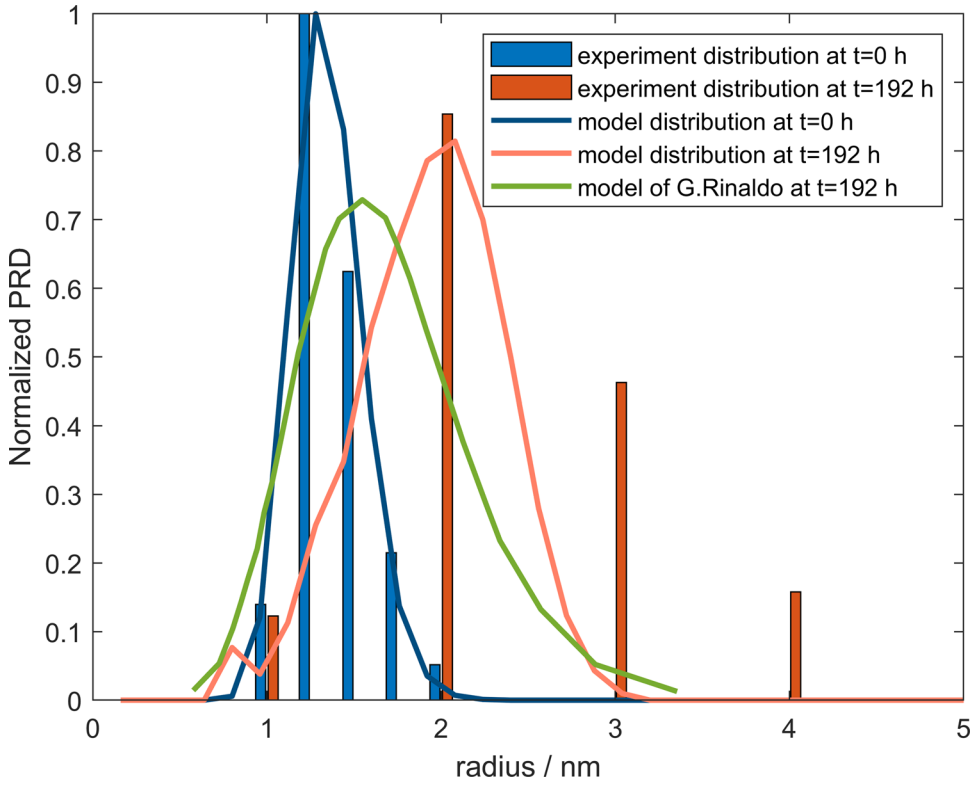

FIGURE 8 Normalized particle radius distribution (PRD) transformation of model and experiment of Wang et al. [43] for platinum (Pt) supported by Vulcan XC-72

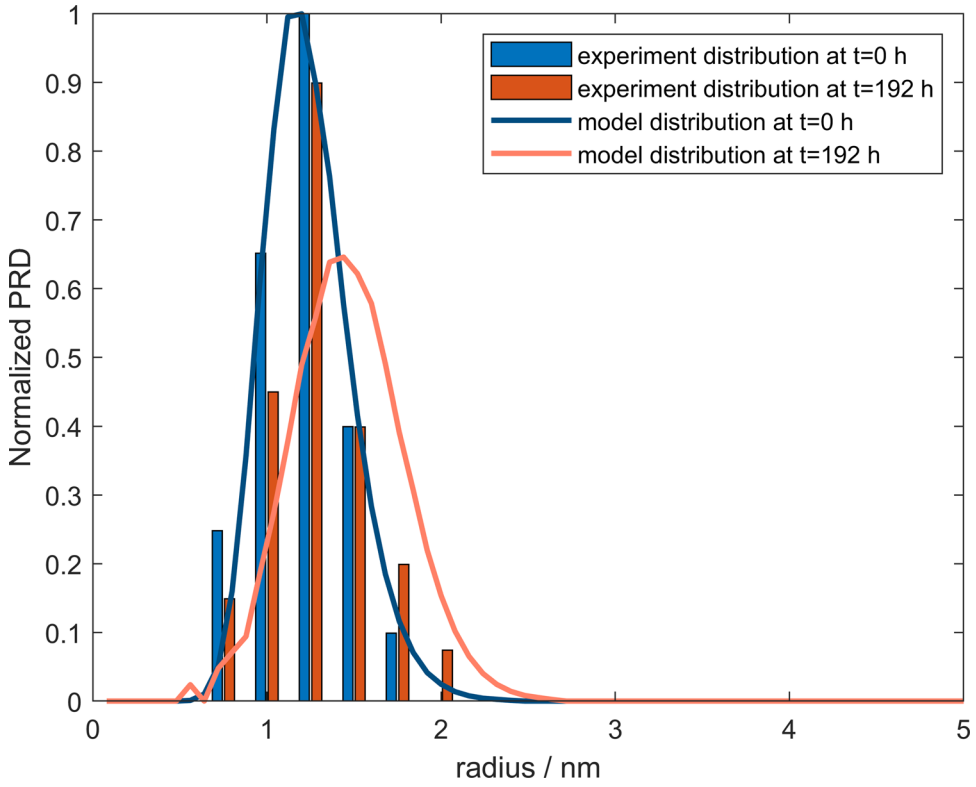

FIGURE 9 Normalized particle radius distribution (PRD) transformation of model and experiment of Wang et al. [43] for Pt supported by multi-walled carbon nanotube (MWNT)

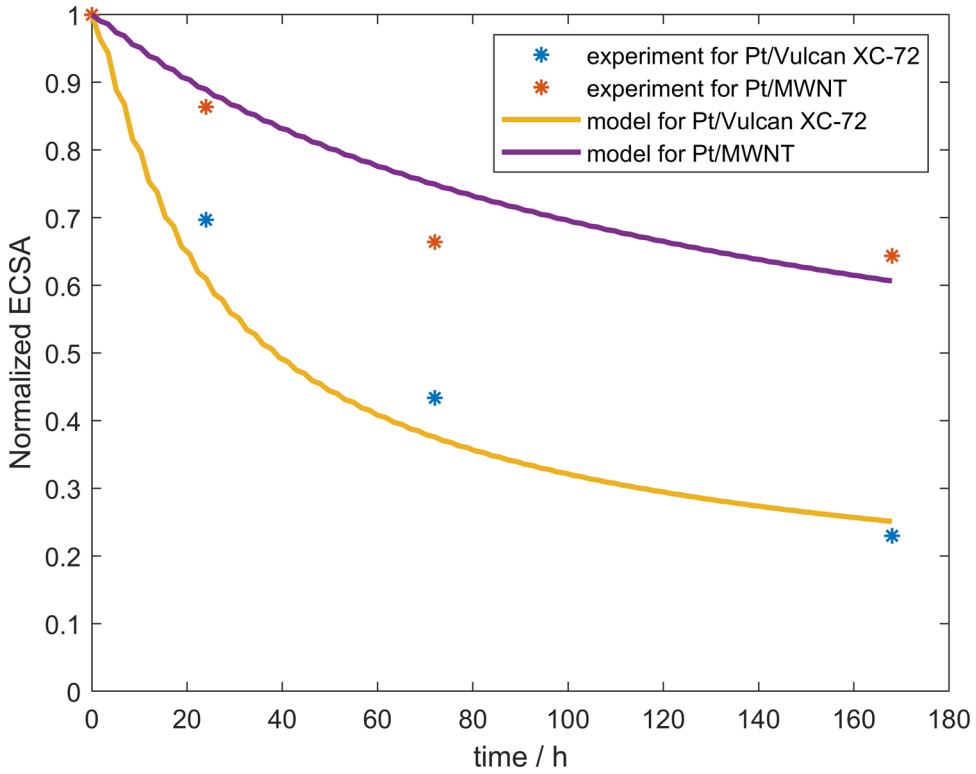

FIGURE 10 Normalized electrochemical surface area (ECSA) of model and experiment of Wang et al. [43] for Pt/Vulcan XC-72 and Pt/MWNT

TABLE 6 Mean electrochemical surface area (ECSA) degradation rate of model and experiment of Wang et al. [43]

Material	Experiment (h^{-1})	Model (h^{-1})	Relative error
Pt/Vulcan XC-72	0.0045848	0.0044573	9.72%
Pt/MWNT	0.0021229	0.0023412	10.28%

The particle size of the model is a little bigger than the experiment after degradation. This may be caused by the difference between the initial PRD of the model and the experiment. As the initial PRD of model does not cover some small particles, the PRD after degradation is also bigger than the experiment. However, the positions of the peaks of the model and the experiment are very close, thus the result is acceptable.

The ECSA was also recorded in the experiment. The comparison between the ECSA of the model and the experiment is shown in Figure 10. The mean degradation rate of the model and the experiment is shown in Table 6. In both experiments, the ECSA of the proposed model and the experiment is close to each other. The relative error of ECSA degradation for both cases is around 10%, which proves that the model is reliable. Also, there are still some differences. For Pt/Vulcan XC-72, the ECSA calculated by the model degrades quicker than the experiment at the beginning, and it can be caused by the effect of strong Ostwald ripening, as it emphasizes the atoms transport between small particles and big particles. For Pt/MWNT, the model result degrades slower than the experiment, and this difference could be caused by the different nature of the support material.

4 | DISCUSSION

The PRD and ECSA of catalyst can only be measured by ex situ experiment, thus it is impossible to detect the fitness of PEMFC catalyst by the experiment during the operation. However, it is necessary and useful to know the health state of catalyst, as it is the basis of PEMFC performance. As has been addressed, the effective surface of catalyst can greatly decide the intensity of oxidation–reduction reactions, thus affects the PEMFC performance and causes catalyst-related fault. Therefore, it is especially important to be aware of the catalyst situation by theory analysis and calculation. Here, we discuss how to apply the proposed model to predict the PEMFC performance degradation.

The proposed model is effective for the calculation of future PRD and ECSA of PEMFC. Thus, it can be applied to estimate the PEMFC performance based on the relationship between the catalyst situation and power

output of PEMFC. Some studies [44] have tried to build the relationship between the ECSA losing and PEMFC power output degradation. For example, the relationship between the power output and electric current of a PEMFC was given under different ECSA in the reference [45], and the power output decreases with the ECSA degradation. However, it is worth noting that the catalyst ECSA loss is severely related to the operation cycles of PEMFC, thus it is not a trivial issue to find the causality between the degradation of catalyst and PEMFC power output. It is out of the scope of this research.

Therefore, for the PEMFC of same batch, the proposed model is able to forecast the catalyst degradation based on the data of one PEMFC. Special experiments can be carried out to provide necessary data for the proposed model, thus the unknown parameters can be obtained by the fitting of the degradation results, then the model can be applied to predict the degradation of other PEMFC. By applying this model, long-term PEMFC catalyst degradation can be predicted by a short-term experiment, thus the experiment duration will be significantly reduced, which is more convenient and more economical.

5 | CONCLUSIONS

Durability is one of the most concerned problems for PEMFC. In this paper, in order to describe the degradation process of PEMFC catalyst, a novel PEMFC catalyst degradation model is proposed for the first time based on catalyst transformation theory, i.e., Pt dissolution and Ostwald coarsening mechanisms. The biggest advantage of the proposed method is that the dynamic transformation of every Pt catalyst particle is directly calculated based on the catalyst transformation theory. The conclusions can be given as follows:

(i) The new PEMFC degradation model can simulate the degradation behavior of Pt catalyst in PEMFC. It is applied to six experimental cases, and the PRD and ECSA result corresponds well with the experiment, which proves that it is reliable.
(ii) The result of the proposed model is more accurate than the analytical model in the reference. The proposed PEMFC catalyst degradation model considers both Pt dissolution and Ostwald ripening mechanisms, thus it is closer to reality.
(iii) This research builds a framework about how to study the transformation process of PEMFC Pt catalyst. With further research about Pt catalyst degradation, more precise mechanisms can be easily added into this model, so that the PEMFC degradation process can be described more clearly and accurately.

For future research, we will try to apply the PEMFC catalyst degradation model to a real PEMFC whose power output is dynamic. By building the relationship between Pt degradation and PEMFC performance, the lifetime of the PEMFC can be predicted. Furthermore, a better power management strategy can be proposed based on this.

ACKNOWLEDGMENTS

The authors gratefully acknowledge the support of this work by the China Scholarship Council (CSC).

ORCID

Kui Chen https://orcid.org/0000-0002-4074-945X

REFERENCES

1. S. Rigal, C. Turpin, A. Jaafar, T. Hordé, J.B. Jollys, N. Chadourne, *Fuel Cells* **2020**, *20*, 272.
2. U. Panchenko, T. Arlt, I. Manke, M. Müller, D. Stolten, W. Lehnert, *Fuel Cells* **2020**, *20*, 300.
3. M. Barakat, B. Tala-Ighil, H. Chaoui, H. Gualous, D. Hissel, *Fuel Cells* **2020**, *20*, 342.
4. J. André, E. Claude, D. Sirac, D. Gastaldin, E. Rossinot, *Fuel Cells* **2020**, *20*, 231.
5. N. Sulaiman, M.A. Hannan, A. Mohamed, E.H. Majlan, W.R. Wan Daud, *Renewable Sustainable Energy Rev.* **2015**, *52*, 802.
6. K. Chen, S. Laghrouche, A. Djerdir, *Fuel Cells* **2020**, *20*, 263.
7. D. Zhang, C. Cadet, N. Yousfi-Steiner, F. Druart, C. Bérenguer, *Fuel Cells* **2017**, *17*, 268.
8. M. Jouin, R. Gouriveau, D. Hissel, M.C. Péra, N. Zerhouni, *Int. J. Hydrogen Energy* **2013**, *38*, 15307.
9. R. Borup, J. Meyers, B. Pivovar, Y.S. Kim, R. Mukundan, N. Garland, D. Myers, M. Wilson, F. Garzon, D. Wood, P. Zelenay, K. More, K. Stroh, T. Zawodzinski, J. Boncella, J.E. McGrath, M. Inaba, K. Miyatake, M. Hori, K. Ota, Z. Ogumi, S. Miyata, A. Nishikata, Z. Siroma, Y. Uchimoto, K. Yasuda, K.-i. Kimijima, N. Iwashita, *Chem. Rev.* **2007**, *107*, 3904.
10. Y. Shao, G. Yin, Y. Gao, *J. Power Sources* **2007**, *171*, 558.
11. X. Yu, S. Ye, *J. Power Sources* **2007**, *172*, 133.
12. X. Yu, S. Ye, *J. Power Sources* **2007**, *172*, 145.
13. A. Marcu, G. Toth, S. Kundu, L.C. Colmenares, R.J. Behm, *J. Power Sources* **2012**, *215*, 266.
14. K. Yu, D. J. Groom, X.Wan, Z Yang, M. Gummalla, S. C. Ball, D. J. Myers, P. J. Ferreira, *Chem. Mater.* **2014**, *26*, 19.
15. C. Takei, K. Kakinuma, K. Kawashima, K. Tashiro, M. Watanabe, M. Uchida, *J. Power Sources*, **2016**, *324*, 729.
16. R.A. Hackendorn, A.V. Virkar, *J. Power Sources* **2013**, *240*, 618.
17. T. Jahnke, G. Futter, A. Latz, T. Malkow, G. Papakonstantinou, G. Tsotridis, P. Schott, M. Gérard, M. Quinaud, M. Quiroga, A.A. Franco, K. Malek, F. Calle-Vallejo, R. Ferreira de Morais, T. Kerber, P. Sautet, D. Loffreda, S. Strahl, M. Serra, P. Polverino, C. Pianese, M. Mayur, W.G. Bessler, C. Kompis, *J. Power Sources* **2016**, *304*, 207.
18. M.C.S. Escaño, *Nano Res.* **2015**, *8*, 1689.
19. L. Tang, X. Li, R.C. Cammarata, C. Friesen, K. Sieradzki, *J. Am. Chem. Soc.* **2010**, *132*, 11722.
20. R. Jinnouchi, E. Toyoda, T. Hatanaka, Y. Morimoto, *J. Phys. Chem. C* **2010**, *114*, 17557.

21. F. Ettingshausen, J. Kleemann, A. Marcu, G. Toth, H. Fuess, C. Roth, *Fuel Cells* **2011**, *11*, 238.
22. Y. Sugawara, A.P. Yadav, A. Nishikata, T. Tsuru, *J. Electroanal. Chem.* **2011**, *662*, 379.
23. S. Cherevko, G.P. Keeley, S. Geiger, A.R. Zeradjanin, N. Hodnik, N. Kulyk, K.J.J. Mayrhofer, *ChemElectroChem* **2015**, *2*, 1471.
24. K. Wettergren, F.F. Schweinberger, D. Deiana, C.J. Ridge, A.S. Crampton, M.D. Rötzer, T.W. Hansen, V.P. Zhdanov, U. Heiz, C. Langhammer, *Nano Lett.* **2014**, *14*, 5803.
25. P.W. Voorhees, *J. Stat. Phys.* **1985**, *38*, 231.
26. R.D. Vengrenovitch, *Acta Metall.* **1982**, *30*, 1079.
27. V.P. Zhdanov, F.F. Schweinberger, U. Heiz, C. Langhammer, *Chem. Phys. Lett.* **2015**, *21*, 631.
28. Q. Wan, S. Hu, J. Dai, C. Chen, W.-X. Li, *J. Phys. Chem. C* **2019**, *123*, 11020.
29. Y.D. Smet, L. Deriemaeker, R. Finsy, *Langmuir* **1997**, *13*, 6884.
30. S.G. Rinaldo, J. Stumper, M. Eikerling, *J. Phys. Chem. C* **2010**, *114*, 5773.
31. R.M. Darling, J.P. Meyers, *J. Electrochem. Soc.* **2003**, *150*, A1523.
32. Z.B. Wang, P.J. Zuo, Y.Y. Chu, Y.Y. Shao, G.P. Yin, *Int. J. Hydrogen Energy* **2009**, *34*, 4387.
33. Z. Xu, H. Zhang, H. Zhong, Q. Lu, Y. Wang, D. Su, *Appl. Catal., B* **2012**, 111–112, *264*.
34. S. Cherevko, N. Kulyk, K.J.J. Mayrhofer, *Nano Energy* **2016**, *29*, 275.
35. A. Baldan, *J. Mater. Sci.* **2002**, *37*, 2379.
36. G.W. Greenwood, *Acta Metall.* **1956**, *4*, 243.
37. I.M. Lifshitz, V.V.J. Slyozov, *J. Phys. Chem. Solids* **1961**, *19*, 35.
38. C. Wagner, *Z. Elektrochem.* **1961**, *65*, 581.
39. J. Wu, X.-Z. Yuan, J.J. Martin, H. Wang, D. Yang, J. Qiao, J. Ma, *J. Power Sources* **2010**, *195*, 1171.
40. Y. Zhang, S. Chen, Y. Wang, W. Ding, R. Wu, L. Li, X. Qi, Z. Wei, *J. Power Sources* **2015**, *273*, 62.
41. P. Parthasarathy, A.V. Virkar, *J. Power Sources* **2013**, *234*, 82.
42. Y. Shao, G. Yin, Y. Gao, P. Shi, *J. Electrochem. Soc.* **2006**, *153*, A1093.
43. X. Wang, W. Li, Z. Chen, M. Waje, Y. Yan, *J. Power Sources* **2006**, *158*, 154.
44. Y. Wang, S.J. Moura, S.G. Advani, A.K. Prasad, *Int. J. Hydrogen Energy* **2019**, *44*, 8479.
45. Y. Ao, S. Laghrouche, D. Depernet, K. Chen, *Int. J. Hydrogen Energy* **2020**, *45*, 32388.

How to cite this article: Y. Ao, K. Chen, S. Laghrouche, D. Depernet. *Fuel Cells*. 2021, 1–15.